Planetary and Space Science xxx (xxxx) xxx

Contents lists available at ScienceDirect

Planetary and Space Science

journal homepage: www.elsevier.com/locate/pss

Phaethon variability during December 2017 closest approach to Earth

M. Lazzarin [a,*], V. Petropoulou [b], I. Bertini [a], F. La Forgia [a], P. Ochner [a,c], A. Migliorini [d], A. Siviero [a]

[a] Department of Physics and Astronomy "G. Galilei", University of Padova, Vicolo dell' Osservatorio 3, I-35122, Padova, Italy
[b] Centro di Ateneo di Studi ed Attivit Spaziali "Giuseppe Colombo" (CISAS), University of Padova, Via Venezia 15, I-35131, Padova, Italy
[c] INAF - Osservatorio Astronomico di Padova, Vicolo Osservatorio 5, I-35122, Padova, Italy
[d] INAF-IAPS, Via del Fosso del Cavaliere n. 100, 00133, Rome, Italy

ARTICLE INFO

Keywords:
Spectroscopy
Asteroids
3200 Phaethon

ABSTRACT

In the course of its last close encounter with the Earth in December 2017, the peculiar Near Earth Object (NEO) 3200 Phaethon has been the target of an international observational campaign in particular connected with the proposed mission Destiny^{+} (Demonstration and Experiment of Space Technology for INterplanetary voYage Phaethon fLyby dUSt science) by JAXA (Japan Aerospace Exploration Agency) to be launched in 2022. The nature of 3200 Phaethon is still debated because of its asteroidal dynamical behavior as opposed to its connection with the Geminid meteor shower, typical cometary residuals. Owing to its vicinity to our planet (Minimum Orbit Intersection Distance MOID = 0.0206 AU) it has been included also in the class of Potentially Hazardous objects and it has been extensively investigated also during its previous perihelion passages. It has been classified as B-type asteroid (Binzel et al., 2001), with different spectral slopes found by several authors in the wavelength region shortward 0.55 μm. Many issues remain to be explored regarding the nature of this object and in this context we observed 3200 Phaethon in the course of 24 h during its last closest approach to the Earth. Low-resolution spectra at very high elevation angles (airmass < 1.15) were acquired with the 1.22–m Asiago telescope on 2017-Dec-16 and 2017-Dec-17. The variation of the viewing geometry during these observations was also derived. We found a significant variation in Phaethon spectral slope in the wavelength range [0.33–0.64] μm during its perigeon passage. The slope varies from $-9.1 \pm 0.2\%(/0.1\mu m)$ on 2017-Dec-16 to $-2.0 \pm 0.1\%(/0.1\mu m)$ on 2017-Dec-17. This variation seems to be related to a disappearing bluer region at high latitudes ($> 70^{\circ}$, close to the North pole). The spectra show also a weak absorption band around 0.43 μm and lack the reflectance downturn at least until $\sim 0.33\mu m$. The comparison with meteorites suggests compositional similarities with CI/CM unusual chondrites. We propose several scenarios that could be responsible for the variability recorded, such as possible surface variations in composition, grain-size, or the level of space weathering and thermal metamorphism. A strong and sudden variation of dust production is also discussed.

1. Introduction

3200 Phaethon is one of the most intriguing Near Earth Objects the origin of which is still debated. A Tisserand invariant with respect to Jupiter of 4.5, combined with a semi-major axis of 1.271 AU, an eccentricity of 0.890 and an inclination of 22.2 deg represent for Phaethon a typical asteroidal orbit. However, its dynamical connection with the Geminid meteor stream (Whipple, 1983), could suggest also some cometary origin for Phaethon even if a cometary activity has never been observed on this object until now.

During the last decade it has been confirmed that Phaethon is an active object, and a dust tail seems recurrent at perihelion (Hui and Li, 2017; Jewitt et al., 2013; Jewitt and Li, 2010), but it is unlikely the result of volatile-driven activity. In fact, owing to a perihelion distance of 0.14 AU, Phaethon reaches a surface temperature up to ~1000 K (Jewitt and Li, 2010): no ice can survive on a body with such a temperature (in agreement with the fact that the Phaethon was found featureless in the 3 μm band by Takir et al., 2018) and this indicates that no ice sublimation can happen as usually seen on comets. On the basis of observations taken from the Solar and Terrestrial Relations Observatory (STEREO) during the perihelion passages in 2009, 2012 and 2016 a dust tail has been revealed and it has been interpreted as the result of thermal fractures and

* Corresponding author.
E-mail address: monica.lazzarin@unipd.it (M. Lazzarin).

https://doi.org/10.1016/j.pss.2018.11.006
Received 28 June 2018; Received in revised form 26 September 2018; Accepted 12 November 2018
Available online xxxx
0032-0633/

decomposition of hydrated silicates, occurring due to the high (~1000 K) temperature present on the surface of the object near perihelion; this mass loss however does not seem enough to maintain the Geminid stream (Hui and Li, 2017; Li and Jewitt, 2013; Jewitt and Li, 2010).

With its Earth MOID (Minimum Orbit Intersection Distance) of 0.0206 AU, Phaethon is also a member of the Potentially Hazardous Asteroids, indeed one of the largest known: Phaethon is 5 km in diameter (Hanuš et al., 2016), or maybe even larger according to newer estimates (Taylor et al., 2018). Several origins have been proposed for Phaethon. A model from Bottke et al. (2002) indicates a more probable origin from the secular resonance ν_6 in the main belt rather than from the Jupiter family or long period comets. de León et al. (2010) suggest an origin from the main belt asteroid Pallas, so it would be a member of its family.

Besides the Geminid stream, Phaethon seems dynamically associated also with other two smaller asteroids: 155140 2005 UD (Ohtsuka et al., 2006; Jewitt and Hsieh, 2006; Kinoshita et al., 2007) and 225416 1999 YC (Kasuga and Jewitt, 2008; Ohtsuka et al., 2008) with which it shares not only similar orbital parameters but also a similar blue color that suggests a similar composition and a possible common origin (Li and Jewitt, 2013).

The surface composition of Phaethon has been studied through visible and infrared spectroscopy (Clark et al., 2010; Licandro et al., 2007) and it has been identified as a B-type asteroid, according to the Bus-DeMeo classification (DeMeo et al., 2009), with a negative slope from the visible wavelengths to the long IR end (~ 2.5μm). The optical spectra, however, show clear slope differences shortward 0.55 μm (see Fig. 4 in Licandro et al., 2007, and references therein). Licandro et al. (2007) state that the variations observed in the UV from the available spectra are larger than the observational uncertainties, noting however that the possible spectral variability has to be confirmed with an homogeneous set of observations (the available spectra were taken during different perihelion passages). The B taxonomic classification determined for Phaethon is quite in contrast with the typical neutral to slightly red spectra of cometary nuclei and Licandro et al. (2007) find also a connection with CI and CM carbonaceous chondrites.

Many open questions remain to be solved regarding the nature, composition and origin of Phaethon, in particular its activity and its behavior in the UV region. During its recent (December 2017) close approach to the Earth, Phaethon has been a target of top importance for ground-based observations, also because of the proposed JAXA's Destiny$^+$ mission to be launched in 2022 (Arai et al., 2018). Another B-type asteroid, 101955 Bennu, will be shortly visited by NASA's OSIRIS-REx with a rendezvous planned for November 2018 and JAXA's Hayabusa2 rendezvous with the Cg-type asteroid 162173 Ryugu (Binzel et al., 2001) is in course (June 2018).

Phaethon closest approach to Earth took place on 2017-Dec-16 at 22:58 UT at a distance of ~0.069 AU. The next close approaches will take place in 2050, 2060, and 2093, at distances 0.083, 0.111, and 0.020 AU respectively.[1] The 2017 encounter was the closest by this asteroid since 1974 and until 2093. We took advantage of this favorable perigeon passage to study Phaethon optical spectra. We performed optical long-slit spectroscopy of Phaethon from the Asiago 1.22-m telescope during the nights 16 December and 17 December 2017. In Section 2 the observations and data reduction procedure are described. In Sections 3 and 4 we present and discuss our results. Section 5 contains the summary and conclusions.

2. Observations

Optical long-slit spectroscopy of Phaethon was carried out during the nights 16 and 17 December 2017 as a target-of-opportunity at the 1.22 m Galileo Telescope of the Department of Physics and Astronomy of the University of Padova in Asiago, Italy (043 IAU code, 45°51′59″ N, 11°31′35″E, h = 1045m). The Boller & Chivens spectrograph was used, equipped with a long-slit with 0.2 mm aperture (corresponding to ~ 3.4″), and a grating of 300 gr/mm giving a nominal dispersion of 2.25 Å/px and spectral coverage of ~ 0.32 − 0.78 μm. The Andor iDus DU440A-BU2 detector was used, with 2048 × 512 px providing a spatial scale of 1″/px. The slit position angle was always set to 0.0° for a better manual tracking of the asteroid motion. The differential refraction due to the atmosphere is estimated to be ~ 1″ at airmass = 1.15 in the near-UV region (Filippenko, 1982), largely included within our slit width of ~ 3.4″. The observing conditions were stable during our observations, with clear sky and seeing ~ 3″.

The spectra were reduced using standard IRAF (Image Reduction and Analysis Facility) routines, as described in Petropoulou et al. (2018). First, the images were trimmed, dark and bias subtracted, and flat-field corrected using lamp flats. The two-dimensional spectra were extracted, sky subtracted, and collapsed to one dimension. Subsequently we corrected for atmospheric extinction. Wavelength calibration was achieved using spectra of He—Fe—Ar comparison lamps. The reflectance spectrum was obtained by dividing the asteroid spectrum with the solar analog star Hyades 64 (Hardorp, 1980) obtained each night at very similar airmass. For our analysis we normalized the spectra at 0.55 μm.

We aimed at following spectroscopically Phaethon rotation, to search for possible surface compositional variation. Phaethon shows bluer than solar colors at $\lambda < 0.4\mu m$, where the atmospheric influence is determinant (through extinction and differential refraction). We thus decided to observe Phaethon at very high elevation angles (airmass < 1.15) to ensure that we are not biased by any systematic errors introduced by atmospheric effects.

Table 1 shows the log of the observations. We present the spectrum name, object observed, time of observation, exposure time, and airmass of the observations. In the last column we report Phaethon rotation phase, at the starting and ending observing time, over the entire period of 3.6 h (Hanuš et al., 2016), assuming as starting point the time of observation of our first spectrum.

The closest approach of the asteroid to Earth took place on 2017-Dec-16 22:58 UT.

3. Results

3.1. Variability of phaethon optical spectra

Fig. 1 shows our observed reflectance spectra, smoothed with a smoothing box-car of 5 pixel. We obtained two spectra on 16 December (spec16_1 in blue at airmass 1.07, and spec16_2 in green at airmass 1.15) and one spectrum on 17 December (spec17 in red, airmass 1.12). These low zenithal distances spectra are almost free from possible biases introduced by atmospheric effects, such as extinction and differential refraction.

We see that the two spectra observed on December 16 (spec16_1 and

Table 1
Observations log. Column 1: Spectrum name. Column 2: Object. Column 3: Time of the observations (UT), in format DATE HH:MM:SS. Column 4: Exposure time (s). Column 5: Airmass. Column 6: Rotation phase at the starting and ending observing time.

NAME	OBJECT	t_{start} (UT)	t_{exp} (s)	airmass	rot. phase
spec16_1	Phaethon	2017-12-16 19:11:54.0	1200.00	1.07	0.0–0.09
spec16_2	Phaethon	2017-12-16 20:11:57.4	1200.00	1.15	0.26–0.35
	Hyades 64	2017-12-16 21:45:58.6	300.00	1.15	
spec17	Phaethon	2017-12-17 17:52:32.6	1200.00	1.12	0.30–0.39
	Hyades 64	2017-12-17 21:37:50.6	200.00	1.15	

[1] http://newton.dm.unipi.it/neodys/index.php?pc=1.1.8&n=3200.

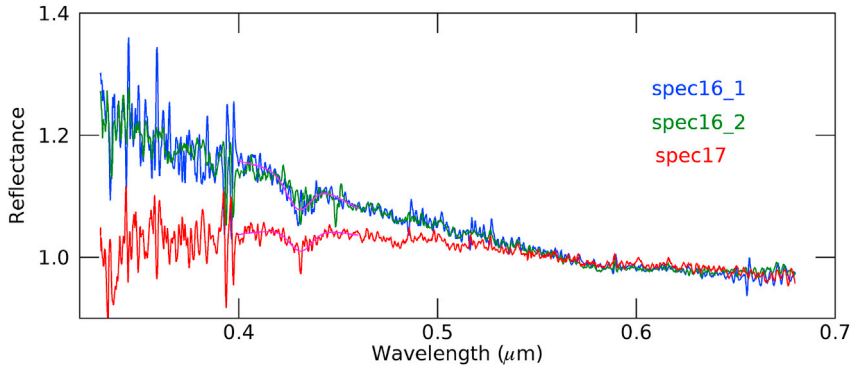

Fig. 1. Phaethon spectra observed during the nights 16 (blue and green) and 17 (red) December 2017. Spectra have been smoothed with a boxcar average of 5 pixel. (For interpretation of the references to color in this figure legend, the reader is referred to the Web version of this article.)

spec16_2) overlap, with a steep and stable negative slope in the wavelength range [0.33–0.58] μm. At 0.58 μm these spectra show a small slope break (close to the small residuals at $\sim 0.589\ \mu m$ introduced by the D ("sodium doublet") solar absorption lines). In the following we average spec16_1 and spec16_2 and we refer to this spectrum as spec16. The spectrum observed on December 17 (spec17), on the other hand, shows a shallower negative slope. It appears slightly flatter at wavelengths shorter than $\sim 0.50\ \mu m$, but in any case, its slope never gets positive. We focus for both spec16 and spec17 on the spectral range [0.33–0.64] μm (free from second-order contamination) and discuss further their difference. At wavelengths larger than 0.64 μm we expect to have second-order contamination (which is present in low-resolution spectra and it is due to the second diffraction order of the blue light), which is expected to be relevant for such a blue reflectance spectrum.

We derive the normalized reflectance slope, or reddening, in units of %/0.1 μm (following Luu and Jewitt, 1990) in the wavelength range [0.33–0.64] μm as:

$$S' = \frac{dS/d\lambda}{S_{\lambda_c}}$$

where S_{λ_c} is the reflectance at 0.55 μm. We use a linear fit that minimizes the chi-square error. The error on the slope measurement has been obtained from the linear fit uncertainty. We find $S'_{16} = -9.1 \pm 0.2\%(/0.1\mu m)$ and $S'_{17} = -2.0 \pm 0.1\%(/0.1\mu m)$.

We note that the derived spectral slopes are meant to quantify the variation of the observed reflectance spectra; however they are not easily comparable with other values present in the literature, as the spectral slope varies significantly depending on the wavelength range and the normalization considered. To illustrate this we derive for our spectra the slope in the wavelength range [0.45–0.65] μm, considered by Luu and Jewitt (1990), and we get $S'_{16} = -6.4 \pm 0.1\%(/0.1\mu m)$ and $S'_{17} = -3.4 \pm 0.1\%(/0.1\mu m)$. These numbers are different from the slopes derived previously in the range [0.33–0.64] μm.

Our data indicate a significant variation in Phaethon spectral slope during its perigeon passage. In Section 4 we examine in detail Phaethon viewing geometry during our observations and we discuss possible causes of the observed variations.

3.2. Spectral features

We note that the cometary emission band due to CN around 0.39 μm, which is an indicator of very volatile cometary ices (Womack et al., 2017), is not present on our spectra. The residuals at 0.393 and 0.397 μm are due to the K and H solar absorption lines.

All our spectra reveal an absorption feature around 0.43 μm, that we highlight in Fig. 1 with magenta curves, drawn from gaussian fits to the features. This weak and wide absorption feature at 0.43 μm was first observed in the reflectance spectra of 13 low-albedo asteroids and it was proposed to be a ferric spin-forbidden absorption in aqueously altered iron-containing minerals (Vilas et al., 1993).

In Fig. 2 we illustrate that the width of the 0.43 μm absorption feature does not correspond to any solar absorption line. In the upper panel we plot Phaethon reflectance spectrum spec16_1 (in blue). The weak absorption feature at 0.43 μm is clearly evident, with a FWHM > 100Å given by a gaussian fit (in magenta). In the lower panel we plot Phaethon (in black) and solar analog Hyades 64 (in red) spectra before division, in

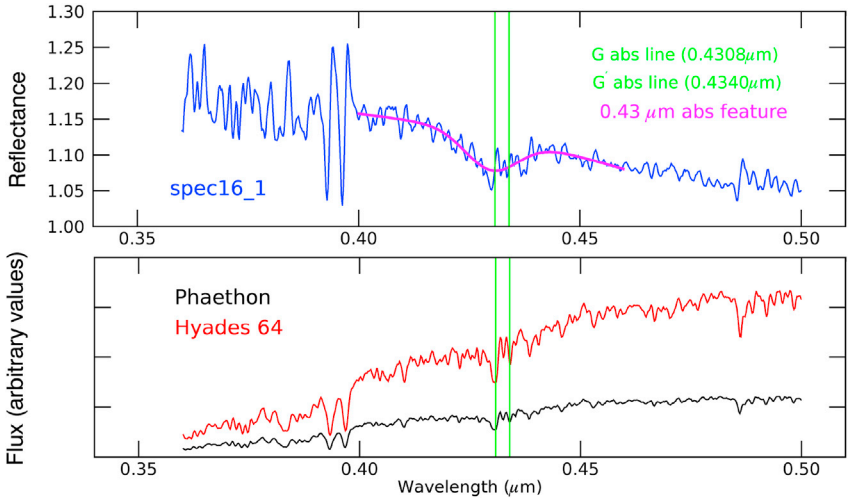

Fig. 2. Upper panel: Phaethon reflectance spectrum spec16_1. The weak absorption feature at 0.43 μm is clearly evident, with a FWHM > 100Å (we fit it with a gaussian curve, indicated by a magenta line). Lower panel: Phaethon (in black) and solar analog Hyades 64 (in red) spectra before division, in arbitrary flux values. The solar absorption lines G (at 0.43079 μm) and G' (at 0.4340 μm), indicated with green lines in both panels, produce narrow and weak residuals at the reflectance spectrum, well differentiated from the 0.43 μm absorption feature. (For interpretation of the references to color in this figure legend, the reader is referred to the Web version of this article.)

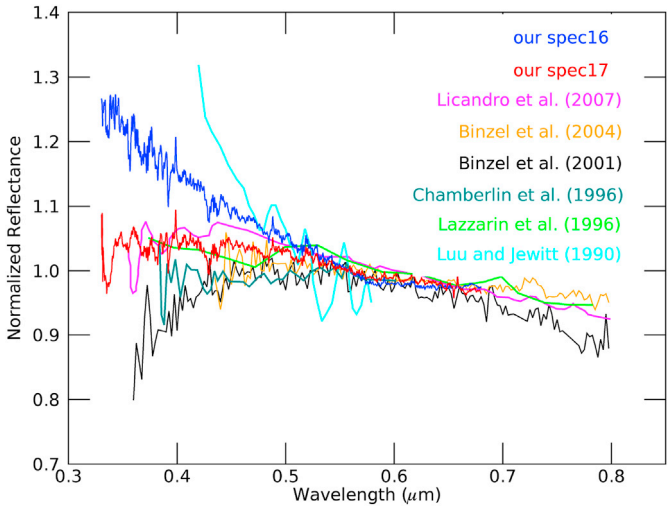

Fig. 3. Comparison of our spectra (spec16 and spec17) obtained during Phaethon closest approach on December 2017, with previously published spectra.

perihelion passage, using an homogeneous set of observations, under stable observing conditions, and using the same solar analog in the two observing nights.

The spectrum presented by Binzel et al. (2001) (provided in digital format in the database http://smass.mit.edu/) shows a reflectance downturn shortward ~ 0.55 μm. Clark et al. (2010) used this spectrum for their analysis of B-Asteroids. Licandro et al. (2007) also reported the reflectance downturn at 0.43 μm, and using models of mineral mixtures they argued that the point of the maximum reflectance can vary with different abundance of hydrated silicates.

It is interesting to note that both our spectra, spec16 and spec17, show linear slopes with no reflectance downturn, at least not until the bluest end of the sampled wavelength range at ~ 0.33 μm. The OSIRIS-REx target asteroid (101955) Bennu, another B-type asteroid, was also found (Clark et al., 2011) to lack the reflectance downturn shortward of ~ 0.48 μm (confirmed by the Eight Color Asteroid Survey (ECAS) photometric data presented by Hergenrother et al., 2013). Clark et al. (2011) discuss the possible origin of this behavior, and they state that variation in the grain size can produce the shifting of the wavelength position of the downturn, with larger grain sizes often exhibiting the start of the reflectance downturn at shorter wavelengths than fine-grained

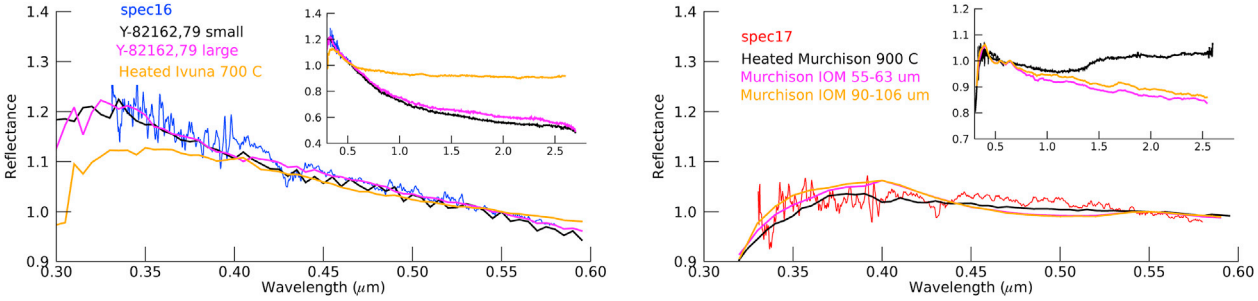

Fig. 4. Comparison of Phaethon optical spectra (left: spectrum observed on 16 December 2017; right: spectrum observed on 17 December 2017) with meteoritic analogs form RELAB database. Large plots show the range [0.33–0.58] μm of our optical spectra, and small inner plots show the whole VIS-NIR wavelength range.

arbitrary flux values. The solar absorption lines G (at 0.43079 μm) and G' (at 0.4340 μm), indicated with green lines in both panels, produce narrow and weak residuals on the reflectance spectrum, well differentiated from the 0.43 μm absorption feature.

This detection, for the first time, of the weak and wide 0.43 μm absorption feature on Phaethon spectra, is discussed further in subsection 4.4.

3.3. Comparison with previously published spectra

Phaethon optical spectra have been presented in previous published works by Licandro et al. (2007); Binzel et al. (2004, 2001); Lazzarin et al. (1996); Chamberlin et al. (1996); Luu and Jewitt (1990). In Fig. 3 we compare the published data with our spectra. We observe that our flatter spectrum spec17 is in good agreement with the spectra presented by Licandro et al. (2007); Binzel et al. (2004, 2001); Lazzarin et al. (1996); Chamberlin et al. (1996). Our bluer spectrum spec16, in turn, shows an intermediate negative slope, comprised within those previous flatter spectra and the steep negative slope spectrum of Luu and Jewitt (1990).

Licandro et al. (2007) also compared their observed spectrum with published data and indicated clear slope differences shortward 0.55 μm, that are larger than the observational uncertainties, but still needing confirmation by an homogeneous set of observations. It is worth noting that all previous spectra were obtained at different perihelion passages and with different observational sets (e.g. instrumentation, solar analog stars etc). Our spectroscopic follow-up confirms, thus, that hinted differences by previous observations are probably real; we have observed the variability of Phaethon reflectance during the December 2017 sample spectra (Johnson and Fanale, 1973; Clark et al., 2010).

3.4. Comparison with meteorites

Licandro et al. (2007) presented a VIS-NIR spectrum of Phaethon covering $0.35 - 2.4 \mu m$ and suggested compositional similarities with aqueously altered CI/CM meteorites and with hydrated silicates such as montmorillonite and antigorite. Among the meteorites, they identified as closer matches all the Yamato-86720 samples and Ivuna heated to 700 °C. They however indicate that the reflectance downturn of these meteoritic spectra occurs at different wavelengths as compared to their observed spectrum. Clark et al. (2010) matched Phaethon VIS-NIR spectrum (presented by DeMeo et al., 2009; Binzel et al., 2001) with CK chondrites and a mineral mix of clorite and carbon.

Here we compare our Phaethon optical spectra (we use the spectral range [0.33–0.58] μm) with the laboratory spectra from the RELAB[2] database using the curve matching methods available in M4AST (mean square error, chi-square, correlation coefficient, and standard deviation of the error; Popescu et al., 2012). In Fig. 4 we plot the first three meteorite spectra that best fit our data, and in Table 2 we resume the results. We have selected the best matches among the carbonaceous chondrites, this general type being well established by the shape of total VIS-NIR spectrum.

Spec16 shows a very good match with Yamato-82162,79 larger and smaller coated chip, the first being the only non-modified meteorite

[2] http://www.planetary.brown.edu/relabdocs/relab.htm.

Table 2
Three meteorite analogs, among the carbonaceous chondrites form RELAB database, that best fit our observed spectra.

Phaethon sp.	Name	Sample ID	Type	Modified	Gr. Size (μm)
spec16	Y-82162,79 smaller coated chip	MB-CMP-019-CA	CC/CI Unusual	Yes	–
	Y-82162,79 larger coated chip	MB-CMP-019-CB	CC/CI Unusual	–	–
	Ivuna Heated 700 °C	MP-TXH-018-E	CC/ Heated CI1	Yes	< 125
spec17	Murchison Heated 900C	MP-TXH-064-HM	CC/CM2	Yes	63 – 125
	Murchison IOM 55–63 um	OG-CMA-004	Org./ CM2	–	55 – 63
	Murchison IOM 90–106 um	OG-CMA-003	Org./ CM2	–	90 – 106

(naturally heated) that has a blue slope. The UV maximum and the preceding downturn of these two samples are in excellent agreement with the observed spectrum (these two meteoritic analogs show slightly different spectral slope in the NIR range, but identical in the optical range that we consider). Another good candidate for the blue spec16 is Ivuna heated at 700 °C with grain-size < 125 μm, but with a slightly shallower slope.

The closest meteoritic analog for spec17 is Murchison heated at 900 °C with grain-size 63–125 μm. Good spectral match is also given by two samples in the RELAB database of high purity organic residuals of Murchison, with grain sizes of 55–63 and 90–106 μm respectively.

Our observed spectra suggest, thus, compositional similarities with CI/CM unusual chondrites, i.e. dehydrated CI/CM chondrites.

4. Discussion

We observe a notable variability of Phaethon spectral slope in the range of our ∼24 h spectroscopic follow-up. Furthermore, we do not observe the reflectance downturn, at least not until 0.33 μm.

4.1. Phaethon viewing geometry

We studied the viewing geometry of the asteroid during our observations in order to ascertain possible causes for the observed spectral variations. We computed the geometry of our observations based on the pole solution by Hanuš et al. (2016) that corresponds to the pole ecliptic coordinates $(\lambda, \beta) = (319^\circ, -39^\circ)$, defining Phaethon north-pole as the sunlit side at the perihelion. Using the NASA ancillary system SPICE kernels and its tools (Acton, 1996; Acton et al., 2018) we computed the sub-Earth latitude, also called aspect angle (see Fig. 5). We also computed the phase angle and the sub-solar point coordinates on the asteroid surface for each epoch. Therefore we estimated the illuminated and visible portion of the asteroid disk (see Fig. 6). The geometric parameters are summarized in Table 3.

In Fig. 7 we show the fraction of Phaethon surface that was actually observed in each observation. We use different colors for the different observations (blue: spec16_1, green: spec16_2, red: spec17). For each observation the subsolar point is represented by the filled circle and the sub-Earth point is represented by the filled square on the map. The area illuminated by the Sun is demarcated by the solid lines, while the area visible from Earth is demarcated by the dotted lines. Thus, the surface on Phaethon, actually observed during each observation is the area comprised within the solid and dotted lines of the same color (comprising also the subsolar and sub-Earth point).

The sub-Earth longitude changes significantly (∼ 100°) from first to second observation, while it changes only 3° between second and third.

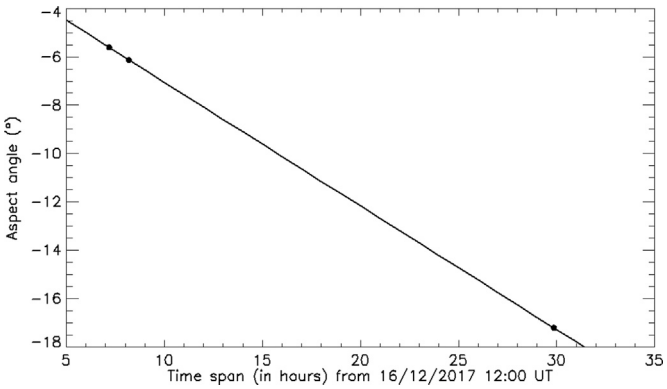

Fig. 5. The aspect angle (i.e. sub-Earth latitude) for our observations on 16 and 17 December 2017, based on the pole solution by Hanuš et al. (2016) with pole ecliptic coordinates $(\lambda, \beta) = (319^\circ, -39^\circ)$.

Between the first and the second observation we are therefore observing significantly different longitudinal regions of the body. The aspect angle (sub-Earth latitude), instead, does not change significantly between the first and the second observation (< 1°) while it changes ∼ 12° between the first and the third observation.

This variation, combined with the solar illumination, implies that in the third observation some regions at high latitudes (> 70°, i.e. close to the north pole, see Fig. 7) disappear from the view. We calculated the variation of the surface observed between the observations spec16_2 and spec17 and found that ∼18% of the observed surface on 16 Dec disappears on 17 Dec, and most of the disappearing surface is found at high latitudes. So the comparison between the spectra obtained during the first and the second night, indicates a possible heterogeneity of the asteroid surface related to the local latitude rather than to the longitude. The drastic change in spectral slope, from −9.1 to −2 (%/0.1μm), hints to a bluer disappearing polar region suggesting to the presence of different material close to the rotational poles of the object with respect to the surface at low or mid latitudes, in agreement with a strongest thermal metamorphism on the north pole region due to a more intense thermal heating (Ohtsuka et al., 2009).

4.2. Variability of phaethon surface properties

Variations in spectral reflectance properties have been attributed by several studies to compositional differences, regolith physical properties (e.g. grain size), varying observing geometries, and space weathering (SpWe) effects. In the following we discuss possible mechanisms for the particular case of Phaethon.

Cloutis et al. (2011) studied the spectral reflectance properties of CI chondrites and found that differences in mineralogy and petrology result in wide variations in spectral properties; in particular, even small differences in composition can cause significant changes in spectral slopes. For example, these authors found that increasing the magnetite abundance results in bluer-sloped spectra; the same trend is observed with variations in the abundance of other materials, such as insoluble organic matter, ferrihydrite, etc. The blueing effect is also produced when increasing the grain size, and Cloutis et al. (2011) note that discriminating among the two mechanisms would be unlikely.

More recently, Cloutis et al. (2018) studied the spectral reflectance properties of Murchison CM2 and found similar trends of its spectral slope as for the CIs. These authors found that small-sized particles (e.g. powder) give redder-sloped spectra (see also Binzel et al., 2015), the spectral properties of powdered samples being affected by both the minimum grain size and average grain size. Correlations of spectral variations with changes in viewing geometry (e.g. phase angle, forward or backscattering etc) were also reported, and the authors conclude that slope variations would not always indicate compositional variations,

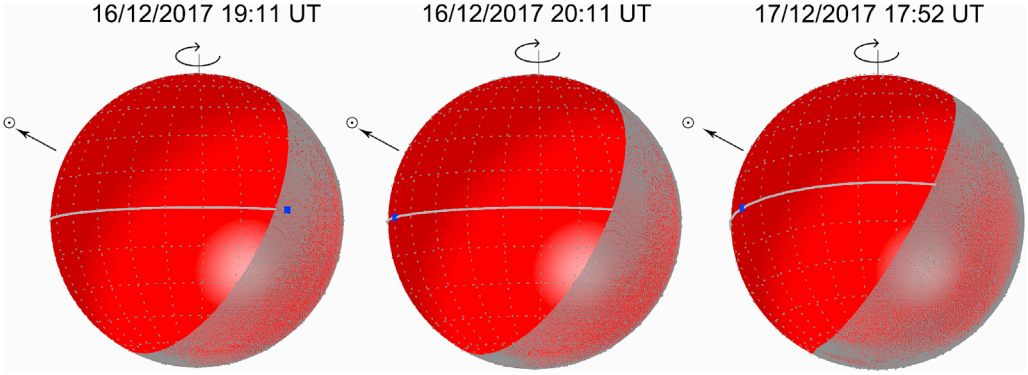

Fig. 6. Geometric reconstruction of the viewing conditions for our 3 Phaethon observations on 16 and 17 December 2017. Hanuš et al. (2016) solution H was used to derive the aspect angle and the subsolar point. The sub-Earth longitude changes significantly from the first to the second observation (∼ 100°) while it changes only 3° between the second and the third. The blue dot on the model shows how a fixed point on the surface of Phaethon would be seen from Earth. Between the first and the second observation we are therefore observing significantly different longitudinal regions of the body. The aspect angle, instead, does not change significantly between the first and the second observation while it changes by about 12° between the first and the third observation. This variation, combined with the solar illumination, implies that in the third observation some regions at high latitudes (> 70°, i.e close to the north pole) disappear from the view. (For interpretation of the references to color in this figure legend, the reader is referred to the Web version of this article.)

Table 3
Phaethon geometric parameters during our observations.

Observation	spec16_1	spec16_2	spec17
Time of obs.	2017-12-16 19:11:54.0	2017-12-16 20:11:57.4	2017-12-17 17:52:32.6
Sub-Earth latitude and longitude	(− 5.61°, 5.53°)	(− 6.14°, − 94.09°)	(− 17.22°, − 91.19°)
subsolar point	(25.7°,-37.5°)	(25.7°,-137.5°)	(25.9°,-143.5°)
phase angle	62.8°	63.4°	76.6°
ill. fraction	73%	72%	62%

especially when the data have strong correlations with topography or they are acquired at high phase angles.

In the light of these works, Phaethon blue-sloped spectra could point to the presence of regions of higher abundance in magnetite, or regions of higher grain size. In Section 4.1 we illustrated that the observed slope variations seem to be linked to variations in the local latitude rather than longitude, in particular the disappearing from the view of surfaces mostly at high latitudes (> 70°, i.e. close to the north pole). The grain size variation scenario is supported by e.g. the close-up images of the small near-Earth asteroid Itokawa (Saito et al., 2006) which evidence a notable diversity of surface morphologies, from boulder fields to smooth areas (at the resolution of the imaging systems).

Alternatively, we explored also the possibility that the slope variation observed could be due to phase reddening effects. In fact, it is well known that spectra of asteroids (Clark et al., 2002), meteorites (Gradie et al., 1980) and comets (Fornasier et al., 2015) can be reddened depending on the phase of o∼bservation and the composition. This effect has been investigated for several taxonomic types of asteroids, and silicate materials seem more influenced by phase reddening effects than primitive carbonaceous materials (Perna et al., 2018). Clark et al. (2011) has investigated insoluble organic matter in the Murchison meteorite and found that it gets bluer at low phase angles (10°) as compared to higher phase angles (50°). Our spectra of Phaethon were obtained at high phase angles (from ∼63 to ∼ 77 degrees, see Table 3), and the difference between the two nights is about 10°, a small variation that can hardly justify the difference in slope that we find. Moreover, on the basis of Lantz et al. (2018), B type asteroid spectral slopes seem poorly influenced by phase reddening effects. Finally, Luu and Jewitt (1990) report that no phase reddening correction is needed beyond 40° phase. However, very little is known on the behavior of B type asteroids with phase reddening in the UV region and more investigation is needed.

Another possible explanation for the observed spectral variations could be the presence of surface alterations due to SpWe. Spectral slope variations caused by SpWe have been considered since many years (e.g. Moroz et al., 2004; Lazzarin et al., 2006; Marchi et al., 2006; Vernazza et al., 2013) producing non definitive trends. In a recent work, Lantz et al. (2017) argue that SpWe effects correlate with the original composition of the carbonaceous chondrite samples, producing reddening (with albedo darkening) to CV and CO classes, and blueing (with brightening) to CM, CI, C2 classes. Lantz et al. (2018) found that surface alterations by SpWe can turn a flat or moderately red spectrum into a negatively sloped B-type, and can move C-type asteroids to B-type. The authors indicate that no evidence is found for reddening of B-type spectra due to SpWe.

Furthermore, Phaethon is a near-Sun asteroid (NSA) and reaches very high surface temperatures of ∼ 1000 K (Jewitt and Li, 2010). Hiroi et al. (1993, 1996) found that solar-radiation heating and in particular the maximum lifetime temperature experienced, can alter spectral properties of carbonaceous chondrites (i.e. thermal metamorphism) producing bluer slopes.

According to Hanuš et al. (2016) thermophysical model, Sun illumination is not connected to a specific area on Phaethon surface at the perihelion passage. Ohtsuka et al. (2009) on the contrary, found a possible inhomogeneity of solar-radiation heating on Phaethon surface, using the pole solution of Krugly et al. (2002). According to their model, the northern mid- and high-latitude regions of Phaethon should be exposed to much higher solar radiation than other regions around the perihelion.

In accordance to this picture, the latitude-dependent slope variations we find in this work would be in agreement with a latitudinally inhomogeneous thermal metamorphism on Phaethon surface, in particular in the northern region, as revealed also by Ohtsuka et al. (2009).

Interestingly, surface color heterogeneity has been reported on asteroid 2005 UD (Kinoshita et al., 2007), considered to be a fragment of Phaethon (Ohtsuka et al., 2006; Jewitt and Hsieh, 2006). Part of its

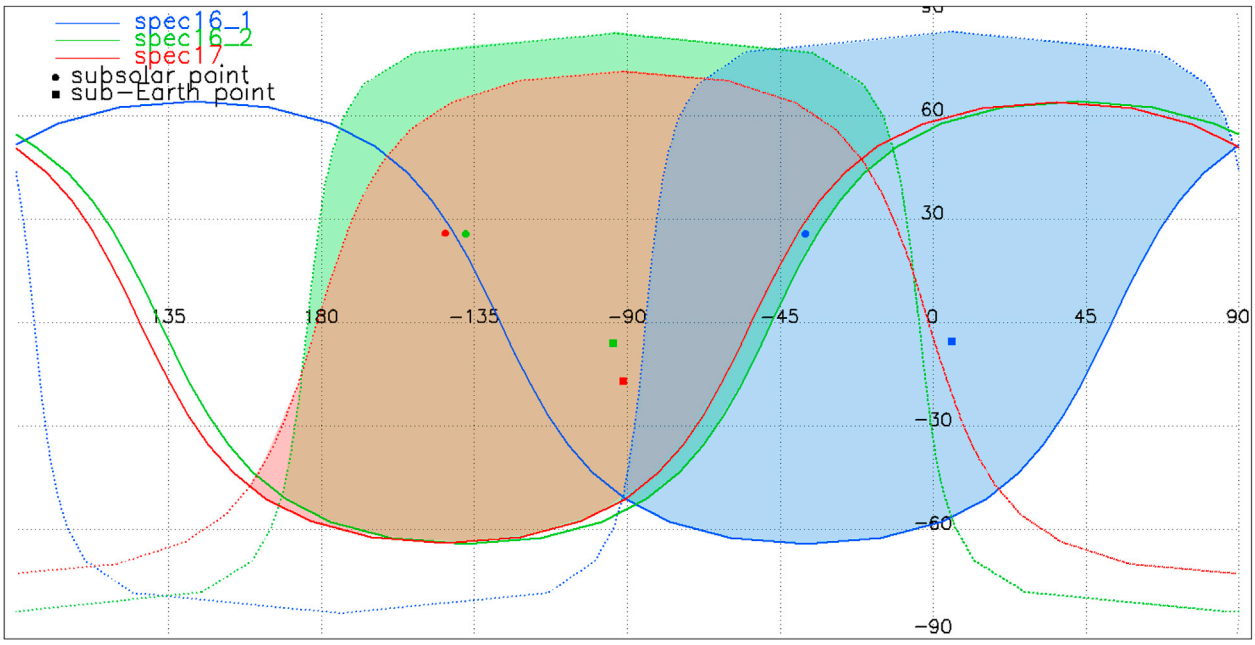

Fig. 7. The fraction of Phaethon surface that was actually observed in each observation. We use different colors for the different observations (blue: spec16_1, green: spec16_2, red: spec17). For each observation the subsolar point is represented by the filled circle and the sub-Earth point is represented by the filled square on the map. The area illuminated by the Sun is demarcated by the solid lines, while the area visible from Earth is demarcated by the dotted lines. Thus, the surface on Phaethon, actually observed during each observation is the area comprised within the solid and dotted lines of the same color. (For interpretation of the references to color in this figure legend, the reader is referred to the Web version of this article.)

surface shows a C-type asteroid colors with flat reflectance, while another part shows bluer reflectance compared to the solar colors, i.e. like an F-type asteroid. The typical bluish slope of F-type asteroids is thought to be the result of the dehydratation of hydrated minerals (Rivkin et al., 2002), implying the C-type surface of 2005 UD would most probably consist of less thermally processed materials.

4.3. Activity caught in the act?

Another scenario, more daring, but plausible, is to attribute the observed variability to Phaethon latent activity. Phaethon is an active asteroid. STEREO observations (Hui and Li, 2017; Jewitt et al., 2013) show that Phaethon releases sub-μm to $\sim 1\mu m$ diameter particles that are producing an anti-solar tail. This dust ejection is also observed as significant brightening (Hui and Li, 2017; Li and Jewitt, 2013) at STEREO images (which have an effective passband centered near 6700 Å with FWHM 1400 Å, approximately the classical photometric R band). Until now Phaethon activity has only been observed at perihelion, when it arrives at an heliocentric distance of 0.14 AU and reaches very high surface temperatures of $\sim$ 1000 K (Jewitt and Li, 2010). Thermal fracture or desiccation cracking at this extreme near-Sun environment are plausible physical mechanisms driving Phaethon activity.

Arendt (2014) detected a dust trail associated with Phaethon orbit using the Cosmic Background Explorer Diffuse Infrared Background Experiment (DIRBE) data (e.g. 12 and 25 μm images). The dust size making up the DIRBE trail would be far larger than the dust tail detected by the STEREO observations. Given that the solar longitude is 264.80 deg (J2000) at the central time of the 1st-night observations, and 265.74 deg at the time of the 2nd-night, and the longitude of ascending node of Phaethon is 265.228 deg, we observed Phaethon under the almost edge-on viewing from the Earth. Therefore, it is possible that either of the spectral observations also detected the Phaethon dust trail. However, this could not explain the observed slope variation between our spectra.

Jewitt (2012) discuss a series of processes (e.g. sublimation, rotational instability, radiation pressure) capable of producing mass loss from a small body that can be effective over heliocentric distances of several AU. A sudden variation of dust production would be compatible with the observed reddening of Phaethon spectrum. Thus, our observations could be interpreted as a first hint that Phaethon could be active (long) before perihelion, during its passage at a $<$ 1AU distance from the Sun (the night of 16–17 December).

The release of fine-grained particles (micron and sub-micron sized) observed at perihelion is not sufficient to account for the Geminid stream in steady-state (Hui and Li, 2017; Li and Jewitt, 2013). Jewitt and Li (2010) proposed that it would be needed $\sim$10 events like these observed, per orbit.

Phaethon activity, caught in the act at 1 AU, would rise questions about the ejection mechanisms, the dust production rate, and the duration of Phaethon activity.

4.4. The spectral feature at 0.43 μm

Our Phaethon spectra reveal, for the first time, a weak and wide absorption feature around 0.43 μm. This absorption band was first detected by Vilas et al. (1993) in the reflectance spectra of 13 low-albedo asteroids and it was ascribed to a ferric spin-forbidden absorption in aqueously altered iron-containing minerals. An absorption band near 0.43 μm is also present in Fe3+-bearing hydrated sulfates (Cloutis et al., 2006) for which it is attributed to Fe3+ spin-forbidden ligand field transitions. Fornasier et al. (2010) also detected a 0.43 μm band in M-type asteroids and argue that it may be associated to chlorites and Mg-rich serpentines or pyroxene minerals such us pigeonite or augite (see also Busarev, 2002, for the detection on M asteroids and a different origin scenario).

The 0.43 μm band was also observed in 21 Lutetia by Lazzarin et al. (2004) and Lazzarin et al. (2010) discuss the possibility that 21 Lutetia high albedo of 0.2 could suggest the presence of metallic materials. Thermal infrared observations (Green et al., 1985; Harris, 1998) suggest that Phaethon optical albedo is 0.11 ± 0.02, a higher albedo than usually found for B type objects. So a similar explanation could fit also Phaethon.

Some attempts have been performed to reveal the presence of aqueous altered materials on Phaethon (see for example Takir et al.,

2018) with negative results and this could be either attributed to the high temperatures reached by the asteroid or to an actual anhydrous nature of the object. However, we have also found a good match with thermally altered carbonaceous chondrites. This finding, connected with very recent determination of low albedo values for Phaethon (Ito et al., 2018), obtained through radiometric observation, and together with the 0.43 μm absorption band determination, could indicate an aqueous altered nature of Phaethon. The conclusion of the possible presence of the 0.43 μm feature points to the peculiar nature of Phaethon and we think that this topic deserves a deep further investigation.

5. Summary and conclusions

Phaethon recent closest encounter with Earth took place on 2017-Dec-16 22:58 UT at a distance of ~ 0.069 AU. During the nights 16 and 17 December we performed a spectroscopic follow-up of Phaethon, using long-slit spectroscopy from 1.22 m Asiago telescope. The spectra were obtained at very high elevation angles (airmass < 1.15) to avoid biases introduced by atmospheric effects (extinction and differential refraction).

Our main results can be summarized as following:

1. Our spectra reveal a significant variation in the UV spectral slope. The slope in the wavelength range [0.33–0.64] μm varies from $S'_{16} = -9.1 \pm 0.2\%(/0.1\mu m)$ on 2017-Dec-16 to $S'_{17} = -2.0 \pm 0.1\%(/0.1\mu m)$ on 2017-Dec-17.
2. Our spectra lack the reflectance downturn at least until $\sim 0.33\mu m$.
3. Our spectra show also a weak absorption band around 0.43 μm.
4. The comparison with meteorites suggest compositional similarities with CI/CM unusual chondrites.
5. The calculation of the viewing geometry during our observations indicate that the slope variability seems to be related to the surfaces disappearing from the view, mostly at high latitudes ($> 70°$, i.e. close to the north pole).
6. We argue that our findings could indicate that either we observe surfaces of different composition, or surfaces covered with grains of different size, or surfaces of different state of SpWe and/or thermal metamorphism. Last, a more daring scenario for the observed spectral variability could be a strong and sudden variation of dust production that could produce a reddening of the spectrum of Phaethon from one night to the other.

Insitu spacecraft measurements from Destiny$^+$ will ascertain whether the observed variability of Phaethon surface properties is due to compositional differences, physical properties, or SpWe effects.

Acknowledgements

V.P. acknowledges the support from the Italian Space Agency by a research grant in the framework of the project Rosetta mission scientific activities and operations support phase E2 (ASI-INAF N. I/024/12/2-2016). IRAF is distributed by the National Optical Astronomy Observatory, which is operated by the Association of Universities for Research in Astronomy (AURA) under a cooperative agreement with the National Science Foundation.

Appendix A. Supplementary data

Supplementary data to this article can be found online at https://doi.org/10.1016/j.pss.2018.11.006.

References

Acton, C., Bachman, N., Semenov, B., Wright, E., Jan. 2018. A Look towards the Future in the Handling of Space Science Mission Geometry, vol. 150, pp. 9–12.

Acton, C.H., Jan. 1996. Ancillary Data Services of NASA's Navigation and Ancillary Information Facility, vol. 44, pp. 65–70.

Arai, T., Kobayashi, M., Ishibashi, K., Yoshida, F., Kimura, H., Wada, K., Senshu, H., Yamada, M., Okudaira, O., Okamoto, T., Kameda, S., Srama, R., Kruger, H., Ishiguro, M., Yabuta, H., Nakamura, T., Watanabe, J., Ito, T., Ohtsuka, K., Tachibana, S., Mikouchi, T., Komatsu, M., Nakamura-Messenger, K., Sasaki, S., Hiroi, T., Abe, S., Urakawa, S., Hirata, N., Demura, H., Komatsu, G., Noguchi, T., Sekiguchi, T., Inamori, T., Yano, H., Yoshikawa, M., Ohtsubo, T., Okada, T., Iwata, T., Nishiyama, K., Toyota, T., Kawakatsu, Y., Takashima, T., Mar. 2018. DESTINY+ mission: flyby of geminids parent asteroid (3200) Phaethon and in-situ analyses of dust accreting on the Earth. In: Lunar and Planetary Science Conference. Vol. 49 of Lunar and Planetary Inst. Technical Report, p. 2570.

Arendt, R.G., Dec. 2014. DIRBE Comet Trails 148, 135.

Binzel, R.P., DeMeo, F.E., Burt, B.J., Cloutis, E.A., Rozitis, B., Burbine, T.H., Campins, H., Clark, B.E., Emery, J.P., Hergenrother, C.W., Howell, E.S., Lauretta, D.S., Nolan, M.C., Mansfield, M., Pietrasz, V., Polishook, D., Scheeres, D.J., Aug. 2015. Spectral Slope Variations for OSIRIS-REx Target Asteroid (101955) Bennu: Possible Evidence for a Fine-grained Regolith Equatorial Ridge, vol. 256, pp. 22–29.

Binzel, R.P., Harris, A.W., Bus, S.J., Burbine, T.H., Jun. 2001. Spectral Properties of Near-earth Objects: Palomar and IRTF Results for 48 Objects Including Spacecraft Targets (9969) Braille and (10302) 1989 ML, vol. 151, pp. 139–149.

Binzel, R.P., Rivkin, A.S., Stuart, J.S., Harris, A.W., Bus, S.J., Burbine, T.H., Aug. 2004. Observed Spectral Properties of Near-Earth Objects: Results for Population Distribution, Source Regions, and Space Weathering Processes, vol. 170, pp. 259–294.

Bottke, W.F., Morbidelli, A., Jedicke, R., Petit, J.-M., Levison, H.F., Michel, P., Metcalfe, T.S., Apr. 2002. Debiased Orbital and Absolute Magnitude Distribution of the Near-earth Objects, vol. 156, pp. 399–433.

Busarev, V.V., Jan. 2002. Hydrated silicates on M-, S-, and E-type Asteroids as possible traces of collisions with bodies from the jupiter growth zone. Sol. Syst. Res. 36, 35–42.

Chamberlin, A.B., McFadden, L.-A., Schulz, R., Schleicher, D.G., Bus, S.J., Jan. 1996. 4015 Wilson-Harrington, 2201 Oljato, and 3200 Phaethon: Search for CN Emission, vol. 119, pp. 173–181.

Clark, B.E., Binzel, R.P., Howell, E.S., Cloutis, E.A., Ockert-Bell, M., Christensen, P., Barucci, M.A., DeMeo, F., Lauretta, D.S., Connolly, H., Soderberg, A., Hergenrother, C., Lim, L., Emery, J., Mueller, M., Dec. 2011. Asteroid (101955) 1999 RQ36: Spectroscopy from 0.4 to 2.4 Mm and Meteorite Analogs, vol. 216, pp. 462–475.

Clark, B.E., Helfenstein, P., Bell, J.F., Peterson, C., Veverka, J., Izenberg, N.I., Domingue, D., Wellnitz, D., McFadden, L., Jan. 2002. NEAR Infrared Spectrometer Photometry of Asteroid 433 Eros, vol. 155, pp. 189–204.

Clark, B.E., Ziffer, J., Nesvorny, D., Campins, H., Rivkin, A.S., Hiroi, T., Barucci, M.A., Fulchignoni, M., Binzel, R.P., Fornasier, S., DeMeo, F., Ockert-Bell, M.E., Licandro, J., Mothé-Diniz, T., Jun. 2010. Spectroscopy of B-type asteroids: subgroups and meteorite analogs. J. Geophys. Res. 115, E06005.

Cloutis, E.A., Hawthorne, F.C., Mertzman, S.A., Krenn, K., Craig, M.A., Marcino, D., Methot, M., Strong, J., Mustard, J.F., Blaney, D.L., Bell, J.F., Vilas, F., Sep. 2006. Detection and Discrimination of Sulfate Minerals Using Reflectance Spectroscopy, vol. 184, pp. 121–157.

Cloutis, E.A., Hiroi, T., Gaffey, M.J., Alexander, C.M.O., Mann, P., Mar. 2011. Spectral Reflectance Properties of Carbonaceous Chondrites: 1. CI Chondrites, vol. 212, pp. 180–209.

Cloutis, E.A., Pietrasz, V.B., Kiddell, C., Izawa, M.R.M., Vernazza, P., Burbine, T.H., DeMeo, F., Tait, K.T., Bell, J.F., Mann, P., Applin, D.M., Reddy, V., May 2018. Spectral Reflectance "deconstruction" of the Murchison CM2 Carbonaceous Chondrite and Implications for Spectroscopic Investigations of Dark Asteroids, vol. 305, pp. 203–224.

de León, J., Campins, H., Tsiganis, K., Morbidelli, A., Licandro, J., Apr. 2010. Origin of the Near-Earth Asteroid Phaethon and the Geminids Meteor Shower, vol. 513, p. A26.

DeMeo, F.E., Binzel, R.P., Slivan, S.M., Bus, S.J., Jul. 2009. An Extension of the Bus Asteroid Taxonomy into the Near-infrared, vol. 202, pp. 160–180.

Filippenko, A.V., Aug. 1982. The Importance of Atmospheric Differential Refraction in Spectrophotometry, vol. 94, pp. 715–721.

Fornasier, S., Clark, B.E., Dotto, E., Migliorini, A., Ockert-Bell, M., Barucci, M.A., Dec. 2010. Spectroscopic Survey of M-type Asteroids, vol. 210, pp. 655–673.

Fornasier, S., Hasselmann, P.H., Barucci, M.A., Feller, C., Besse, S., Leyrat, C., Lara, L., Gutierrez, P.J., Oklay, N., Tubiana, C., Scholten, F., Sierks, H., Barbieri, C., Lamy, P.L., Rodrigo, R., Koschny, D., Rickman, H., Keller, H.U., Agarwal, J., A'Hearn, M.F., Bertaux, J.-L., Bertini, I., Cremonese, G., Da Deppo, V., Davidsson, B., Debei, S., De Cecco, M., Fulle, M., Groussin, O., Güttler, C., Hviid, S.F., Ip, W., Jorda, L., Knollenberg, J., Kovacs, G., Kramm, R., Kührt, E., Küppers, M., La Forgia, F., Lazzarin, M., Lopez Moreno, J.J., Marzari, F., Matz, K.-D., Michalik, H., Moreno, F., Mottola, S., Naletto, G., Pajola, M., Pommerol, A., Preusker, F., Shi, X., Snodgrass, C., Thomas, N., Vincent, J.-B., Nov. 2015. Spectrophotometric Properties of the Nucleus of Comet 67P/Churyumov-gerasimenko from the OSIRIS Instrument Onboard the ROSETTA Spacecraft, vol. 583, p. A30.

Gradie, J.C., Veverka, J., Buratti, B.J., Mar. 1980. The effects of photometric geometry on spectral reflectance. In: Lunar and Planetary Science Conference. Vol. 11 of Lunar and Planetary Inst. Technical Report, pp. 357–359.

Green, S.F., Meadows, A.J., Davies, J.K., Jun. 1985. Infrared Observations of the Extinct Cometary Candidate Minor Planet (3200) 1983TB, vol. 214, pp. 29P–36P.

Hanuš, J., Delbo, M., Vokrouhlický, D., Pravec, P., Emery, J.P., Alí-Lagoa, V., Bolin, B., Devogèle, M., Dyvig, R., Galád, A., Jedicke, R., Kornoš, L., Kušnirák, P., Licandro, J., Reddy, V., Rivet, J.-P., Világi, J., Warner, B.D., Jul. 2016. Near-Earth Asteroid (3200)

Phaethon: Characterization of its Orbit, Spin State, and Thermophysical Parameters, vol. 592, p. A34.
Hardorp, J., Aug. 1980. The sun among the stars. II - solar color. Hyades metal content, and distance 88, 334–344.
Harris, A.W., Feb. 1998. A Thermal Model for Near-earth Asteroids, vol. 131, pp. 291–301.
Hergenrother, C.W., Nolan, M.C., Binzel, R.P., Cloutis, E.A., Barucci, M.A., Michel, P., Scheeres, D.J., d'Aubigny, C.D., Lazzaro, D., Pinilla-Alonso, N., Campins, H., Licandro, J., Clark, B.E., Rizk, B., Beshore, E.C., Lauretta, D.S., Sep. 2013. Lightcurve, Color and Phase Function Photometry of the OSIRIS-REx Target Asteroid (101955) Bennu, vol. 226, pp. 663–670.
Hiroi, T., Pieters, C.M., Zolensky, M.E., Lipschutz, M.E., Aug. 1993. Evidence of thermal metamorphism on the C, G, B, and F asteroids. Science 261, 1016–1018.
Hiroi, T., Zolensky, M.E., Pieters, C.M., Lipschutz, M.E., May 1996. Thermal metamorphism of the C, G, B, and F asteroids seen from the 0.7 micron, 3 micron and UV absorption strengths in comparison with carbonaceous chondrites. Meteoritics Planet Sci. 31, 321–327.
Hui, M.-T., Li, J., Jan. 2017. Resurrection of (3200) Phaethon in 2016, vol. 153, p. 23.
Ito, T., Ishiguro, M., Arai, T., Imai, M., Sekiguchi, T., Bach, Y.P., Kwon, Y.G., Kobayashi, M., Ishimaru, R., Naito, H., Watanabe, M., Kuramoto, K., Jun. 2018. Extremely strong polarization of an active asteroid (3200) Phaethon. Nat. Commun. 9, 2486.
Jewitt, D., Mar. 2012. The Active Asteroids 143, 66.
Jewitt, D., Hsieh, H., Oct. 2006. Physical Observations of 2005 UD: a Mini-Phaethon, vol. 132, pp. 1624–1629.
Jewitt, D., Li, J., Nov. 2010. Activity in Geminid Parent (3200) Phaethon, vol. 140, pp. 1519–1527.
Jewitt, D., Li, J., Agarwal, J., Jul. 2013. The Dust Tail of Asteroid (3200) Phaethon, vol. 771, p. L36.
Johnson, T.V., Fanale, F.P., 1973. Optical Properties of Carbonaceous Chondrites and Their Relationship to Asteroids, vol. 78, pp. 8507–8518.
Kasuga, T., Jewitt, D., 2008. Observations of 1999 YC and the Breakup of the Geminid Stream Parent, vol. 136, pp. 881–889.
Kinoshita, D., Ohtsuka, K., Sekiguchi, T., Watanabe, J., Ito, T., Arakida, H., Kasuga, T., Miyasaka, S., Nakamura, R., Lin, H.-C., May 2007. Surface Heterogeneity of 2005 UD from Photometric Observations, vol. 466, pp. 1153–1158.
Krugly, Y.N., Belskaya, I.N., Shevchenko, V.G., Chiorny, V.G., Velichko, F.P., Mottola, S., Erikson, A., Hahn, G., Nathues, A., Neukum, G., Gaftonyuk, N.M., Dotto, E., Aug. 2002. The Near-earth Objects Follow-up Program. IV. CCD Photometry in 1996-1999, vol. 158, pp. 294–304.
Lantz, C., Binzel, R.P., DeMeo, F.E., Mar. 2018. Space Weathering Trends on Carbonaceous Asteroids: a Possible Explanation for Bennu's Blue Slope?, vol. 302, pp. 10–17.
Lantz, C., Brunetto, R., Barucci, M.A., Fornasier, S., Baklouti, D., Bourçois, J., Godard, M., Mar. 2017. Ion Irradiation of Carbonaceous Chondrites: a New View of Space Weathering on Primitive Asteroids, vol. 285, pp. 43–57.
Lazzarin, M., Barucci, M.A., Doressoundiram, A., Jul. 1996. Visible Spectroscopy of Possible Cometary Candidates, vol. 122, pp. 122–127.
Lazzarin, M., Magrin, S., Marchi, S., Dotto, E., Perna, D., Barbieri, C., Barucci, M.A., Fulchignoni, M., Nov. 2010. Rotational Variation of the Spectral Slope of (21) Lutetia, the Second Asteroid Target of ESA Rosetta Mission, vol. 408, pp. 1433–1437.
Lazzarin, M., Marchi, S., Magrin, S., Barbieri, C., Oct. 2004. Visible spectral properties of asteroid 21 Lutetia. target of Rosetta Mission 425, L25–L28.
Lazzarin, M., Marchi, S., Moroz, L.V., Brunetto, R., Magrin, S., Paolicchi, P., Strazzulla, G., Aug. 2006. Space Weathering in the Main Asteroid Belt: the Big Picture, vol. 647, pp. L179–L182.
Li, J., Jewitt, D., Jun. 2013. Recurrent Perihelion Activity in (3200) Phaethon, vol. 145, p. 154.
Licandro, J., Campins, H., Mothé-Diniz, T., Pinilla-Alonso, N., de León, J., Jan. 2007. The Nature of Comet-asteroid Transition Object (3200) Phaethon, vol. 461, pp. 751–757.
Luu, J.X., Jewitt, D.C., Jun. 1990. Charge-coupled Device Spectra of Asteroids. I - Near-earth and 3:1 Resonance Asteroids, vol. 99, pp. 1985–2011.
Marchi, S., Paolicchi, P., Lazzarin, M., Magrin, S., Feb. 2006. A General Spectral Slope-exposure Relation for S-type Main Belt and Near-earth Asteroids, vol. 131, pp. 1138–1141.
Moroz, L., Baratta, G., Strazzulla, G., Starukhina, L., Dotto, E., Barucci, M.A., Arnold, G., Distefano, E., Jul. 2004. Optical Alteration of Complex Organics Induced by Ion Irradiation:. 1. Laboratory Experiments Suggest Unusual Space Weathering Trend, vol. 170, pp. 214–228.
Ohtsuka, K., Arakida, H., Ito, T., Yoshikawa, M., Asher, D.J., Aug. 2008. Apollo Asteroid 1999 YC: Another Large Member of the PGC? Meteoritics and Planetary Science Supplement, vol. 43, p. 5055.
Ohtsuka, K., Nakato, A., Nakamura, T., Kinoshita, D., Ito, T., Yoshikawa, M., Hasegawa, S., Dec. 2009. Solar-radiation Heating Effects on 3200 Phaethon, vol. 61, pp. 1375–1387.
Ohtsuka, K., Sekiguchi, T., Kinoshita, D., Watanabe, J.-I., Ito, T., Arakida, H., Kasuga, T., May 2006. Apollo Asteroid 2005 UD: Split Nucleus of (3200) Phaethon?, vol. 450, pp. L25–L28.
Perna, D., Barucci, M.A., Fulchignoni, M., Popescu, M., Belskaya, I., Fornasier, S., Doressoundiram, A., Lantz, C., Merlin, F., Aug. 2018. A Spectroscopic Survey of the Small Near-Earth Asteroid Population: Peculiar Taxonomic Distribution and Phase Reddening, vol. 157, pp. 82–95.
Petropoulou, V., Lazzarin, M., Bertini, I., Ochner, P., Forgia, F.L., Siviero, A., Ferri, F., Naletto, G., 2018. Spectroscopic observations of the bilobate potentially hazardous asteroid 2014 jo25 from the asiago 1.22-m telescope. Planet. Space Sci. 158, 63–68. http://www.sciencedirect.com/science/article/pii/S0032063318300205.
Popescu, M., Birlan, M., Nedelcu, D.A., Aug. 2012. Modeling of Asteroid Spectra - M4AST, vol. 544, p. A130.
Rivkin, A.S., Howell, E.S., Vilas, F., Lebofsky, L.A., Mar. 2002. Hydrated Minerals on Asteroids: the Astronomical Record, pp. 235–253.
Saito, J., Miyamoto, H., Nakamura, R., Ishiguro, M., Michikami, T., Nakamura, A.M., Demura, H., Sasaki, S., Hirata, N., Honda, C., Yamamoto, A., Yokota, Y., Fuse, T., Yoshida, F., Tholen, D.J., Gaskell, R.W., Hashimoto, T., Kubota, T., Higuchi, Y., Nakamura, T., Smith, P., Hiraoka, K., Honda, T., Kobayashi, S., Furuya, M., Matsumoto, N., Nemoto, E., Yukishita, A., Kitazato, K., Dermawan, B., Sogame, A., Terazono, J., Shinohara, C., Akiyama, H., Jun. 2006. Detailed images of asteroid 25143 Itokawa from Hayabusa. Science 312, 1341–1344.
Takir, D., Reddy, V., Hanus, J., Arai, T., Lauretta, D.S., Kareta, T., Howell, E.S., Emery, J.P., McGraw, L.E., Mar. 2018. 3-m spectroscopy of asteroid (3200) Phaethon: implications for B-asteroids. In: Lunar and Planetary Science Conference. Vol. 49 of Lunar and Planetary Inst. Technical Report, p. 2624.
Taylor, P.A., Marshall, S.E., Venditti, F., Virkki, A.K., Benner, L.A.M., Brozovic, M., Naidu, S.P., Howell, E.S., Kareta, T.R., Reddy, V., Takir, D., Rivkin, A.S., Zambrano-Marin, L.F., Bhiravarasu, S.S., Rivera-Valentin, E.G., Aponte-Hernandez, B., Rodriguez Sanchez-Vahamonde, C., Nolan, M.C., Giorgini, J.D., Vervack, R.J., Fernandez, Y.R., Crowell, J.L., Lauretta, D.S., Arai, T., Mar. 2018. Radar and infrared observations of near-earth asteroid 3200 Phaethon. In: Lunar and Planetary Science Conference. Vol. 49 of Lunar and Planetary Inst. Technical Report, p. 2509.
Vernazza, P., Fulvio, D., Brunetto, R., Emery, J.P., Dukes, C.A., Cipriani, F., Witasse, O., Schaible, M.J., Zanda, B., Strazzulla, G., Baragiola, R.A., Jul. 2013. Paucity of Tagish Lake-like Parent Bodies in the Asteroid Belt and Among Jupiter Trojans, vol. 225, pp. 517–525.
Vilas, F., Hatch, E.C., Larson, S.M., Sawyer, S.R., Gaffey, M.J., Apr. 1993. Ferric Iron in Primitive Asteroids - a 0.43-micron Absorption Feature, vol. 102, pp. 225–231.
Whipple, F.L., Oct. 1983. 1983 TB and the Geminid Meteors, p. 3881.
Womack, M., Sarid, G., Wierzchos, K., Mar. 2017. CO in Distantly Active Comets, vol. 129, p. 031001 (3).